Electronic Supplementary Material (ESI) for Chemical Communications

SUPPORTING MATERIAL

Antimicrobial Metallopeptides with Broad Nuclease and Ribonuclease Activity

Jeff C. Joyner,[a,b,c] W. F. Hodnick,[c] Ada S. Cowan,[c] Deepika Tamuly,[c] Rachel Boyd,[c] and J. A. Cowan[a,b,c,d] *

Contribution from [a] Evans Laboratory of Chemistry, Ohio State University, 100 West 18th Avenue, Columbus, Ohio 43210; [b] The Ohio State Biochemistry Program, 784 Biological Sciences 484 W. 12th Avenue, Columbus, Ohio 43210; and [c] MetalloPharm LLC, 1790 Riverstone Drive, Delaware, OH 43015; [d] The Ohio State University Center for RNA Biology, USA

Table of Contents for Supporting Information

Materials and Methods

Materials. All peptides were purchased from Aapptec, and concentrations were determined by both UV/Vis spectroscopy and Ni(II) ion titrations, in the same manner as done previously.[1-3] The custom RNA constructs Fl-RRE IIB RNA, with sequence 5'-fluorescein-UUGGUCUGGGCGCAGCGCAAG CUGACGGUACAGGCC-3', Fl-16S A-site RNA, with sequence 5'-fluorescein-GGCGUCACACCUU CGGGUGAAGUCGCC-3', Fl-HCV IV RNA, with sequence 5'-fluorescein-GGACCGUGCACCAUG AGCACGAAUCC-3', and Fl-HCV IIB RNA, with sequence 5'-fluorescein-GGCAGAAAGCGUCUA GCCAUGGCGUUAGUAUGCC-3', were purchased from Dharmacon. Cu(II) chloride dihydrate and Ni(II) acetate tetrahydrate were purchased from J.T. Baker and Aldrich, respectively. TCEP-HCl was purchased from Thermo Scientific. Sodium chloride and sodium hydroxide were purchased from Fisher, and HEPES was purchased from Sigma.

DNA-binding titrations. Dissociation constants (K_D) for binding of peptides/complexes by plasmid DNA were determined by fluorimetry by use of a fluorescence spectrophotometer (Varian Cary Eclipse) with excitation at 280 nm (SW = 5 nm) and monitoring tryptophan emission at both 328 nm and 362 nm (SW = 10 nm). A 500 μL volume of 1 μM peptide or complex was added to the pre-thermostatted cuvette, at the titration temperature (37 °C). After 10 min of temperature equilibration, a solution containing 40 μM base pairs pUC19 plasmid DNA (supercoiled form) was titrated into the solution. After each addition, the solution was mixed by gentle pipetting, allowed to equilibrate for 3 min, and the ratio of the fluorescence intensity at 362 nm to that at 328 nm was recorded—this provided a measure of the blue shift in tryptophan fluorescence maximum that occurred upon DNA-binding by peptide or complex. Dilution-corrected, normalized titration response curves were fit to the binding equation shown by equation (1), where F_{obs} is the observed ratio of fluorescence intensities listed above, D_0 is the total concentration of added DNA (μM base pairs), F_P and F_{PD} are fitting parameters corresponding to the ratios of fluorescence intensities at the wavelengths listed above for the unbound and DNA-bound peptide, respectively, P_0 is the initial concentration of peptide, and K_D is the fitted dissociation constant. All binding experiments were performed in a binding buffer composed of 20 mM HEPES, 100 mM NaCl, pH 7.

$$F_{obs} = F_P + \{K_D + P_0 + D_0 - [(K_D + P_0 + D_0)^2 - (4 \cdot P_0 \cdot D_0)]^{1/2}\}(F_{PD} - F_P)/(2 \cdot P_0) \quad (1)$$

RNA-binding titrations. Dissociation constants (K_D) for binding of each fluorescein-labeled stem loop RNA by peptides/complexes were determined by fluorimetry on a Varian Cary Eclipse fluorescence spectrophotometer, with excitation at 494 nm (SW = 5 nm) and emission at 525 nm (SW = 5 nm). A 660 μL volume of 100 nM AP-RRE RNA was first heated to 90 °C for 5 min and then allowed to cool to, but not below, the titration temperature (37 °C). A 650 μL volume of this sample was added to the pre-thermostatted cuvette. After 10 min of temperature equilibration a solution of 100 μM peptide or complex was titrated into the solution. After each addition, the solution was mixed by gentle pipetting to ensure complete mixing. The fluorescence change associated with the change of environment of the fluorescein label was monitored following peptide binding. Dilution-corrected, normalized titration response curves (F_{obs} vs [peptide]) were fit to the binding equation shown by equation (2), where [peptide] is the concentration of peptide or complex and n is the apparent stoichiometry of binding, in order to obtain a fitted dissociation constant (K_D). All binding experiments were performed in a binding buffer composed of 20 mM HEPES, 100 mM NaCl, pH 7.

$$F_{obs} = 1/[1 + ([peptide]/K_D)^n] \quad (2)$$

DNA cleavage kinetics. Reactions were run aerobically with 20 µL of 10 µM base pair pUC19, 100 nM complex or peptide, and 1 mM co-reactants (H_2O_2 and/or ascorbate) in 20 mM HEPES, 100 mM NaCl, pH 7. After 4 h incubation, the reactions were quenched simultaneously by placing on ice and adding loading dye (bromophenol blue in sucrose solution). The quenched reactions were immediately loaded onto 1% agarose gel containing ethidium bromide, separated for 30-45 min at 120 V, and visualized using a BioRad gel doc. Remaining supercoiled, nicked, and linearized plasmid DNA was quantified for each reaction with the program ImageQuant. A correction factor of 1.47 was applied for the intensity of supercoiled DNA to account for the diminished ability of supercoiled DNA to intercalate ethidium bromide.

RNA cleavage kinetics. Reactions of 1 µM complex (1:1.5 Cu:peptide ratio), 1 µM of each 5‘ fluorescein end-labeled RNA, and 1 mM co-reactants (H_2O_2 and/or ascorbate) were conducted at 37 °C in separate tubes, each containing 20 µL total reaction volume – one tube corresponding to one gel lane. A buffer consisting of 20 mM HEPES, 100 mM NaCl, pH 7 was used in all experiments. Prior to reaction, each fluorescein-labeled RNA was heated to 90 °C and allowed to cool to, but not below 37 °C, and RNA was immediately added to each pre-incubated tube. Reactants were added to pre-incubated tubes (37 °C) to start the reactions, which proceeded for 5.5 h in a dark incubator. To quench, a 4 µL aliquot from each reaction added to 196 µL of a quenching/gel-loading buffer solution consisting of standard 1x tris-EDTA-acetic acid buffer, 8M urea, 20 mM HEPES, 100 mM NaCl. The tubes were then heated to 90 °C for 5 min, and a 5 µL aliquot from each tube was then loaded into its corresponding lane of a 10% polyacrylamide 8 M urea gel. Gel electrophoresis was performed at 250 V for 1.5 h. Gels were analyzed on a GE Typhoon variable mode imager using 488 nm excitation and a 526 nm single pass emission filter. Bands were quantified with the program ImageQuant. For each reaction, the remaining concentration of full-length RNA was determined.

MALDI-TOF mass spectrometry analysis of RNA-cleavage kinetics. Cleavage reactions were quenched by placement on ice and immediately desalted. C_{18} zip-tips were used for desalting, with initial wetting by 50/50 acetonitrile/water and pre-equilibration with 2M triethylamine acetate, followed by loading of quenched RNA reaction mixtures onto the zip-tips. The RNA that was bound to each zip-tip was washed first 3 times with 2M triethylamine acetate and then 3 times with nanopure water. Elution of RNA from zip-tips was performed using 5 µL ice cold 50/50 acetonitrile/water. Each desalted RNA product mixture, in 5 µL 50/50 acetonitrile/water, was mixed with 2.5 µL of a matrix solution containing 42 mg/mL 3-hydroxypicolinic acid, 6.8 mg/mL ammonium citrate in 30/70 acetonitrile/water. Each target on a Bruker ground steel 96 target microScout plate was spotted using a two-layer approach, where each target was first pre-spotted with 1 µL of the matrix solution and allowed to dry, before spotting with 2.5 µL of the above RNA/matrix mixture and again allowed to dry. A desalted calibration mixture containing 3 separate RNA species of varying molecular weights bracketing the range of m/z studied was used to calibrate the instrument prior to each analysis; the calibration mixture was spotted on a separate target on the same plate, and in the same manner, as all other RNA mixtures. All MALDI-TOF MS analysis was performed on a Bruker MicroFlex LRF instrument, equipped with a gridless reflectron, using negative ion and reflectron modes. The pulsed ion extraction time was 1200 ns. At least 1000 shots were summed per spectrum. Using Bruker flexAnalysis software, spectra were smoothed using a Savitzgy-Golay algorithm. Internal calibrations

of spectra were performed using a set of regularly-occurring fragmentation and/or doubly-charged full-length RNA peaks, and a peak list was generated for each spectrum that contained m/z values and peak areas. Peak mass-matching was performed using our internally developed MassDaddy Perl script, written by Jeff C. Joyner, that requires user input of a matching tolerance (ppm) and two input files: (1) an expected-mass list file containing all expected RNA cleavage fragments (all positions combined with all overhang types) and corresponding masses; (2) a peak list with all observed masses and respective peak areas. Assignment of peaks was performed by comparison of each peak list with the theoretical masses for all expected cleavage products, with a matching tolerance of 200 ppm. MassDaddy creates one output file for each mass spectrum, with six columns: the theoretical m/z (Da), the observed m/z (Da), the mass matching error (ppm), the nucleotide position of the nascent overhang, the nascent overhang type, and the peak area, arranged by overhang type and sequence. Only peaks with m/z > 1000 amu were considered in this study, since excessive spectral crowding occurred at lower m/z ranges. Following automated mass-matching of peaks, the peak areas of all mass-matched peaks were summed, and the peak area fraction for each peak was determined; only peaks with a peak area fraction above a threshold of 0.0005 were considered (Supporting Information). For time-dependent reactions, the change in peak area fraction (semi-quantitative mole fraction) for each species over time was fit to a first order model, and semi-quantitative apparent initial rates (nM/min) were determined. More detail on the methodology can be found elsewhere.[4]

Bacterial growth inhibition assays. Bacterial minimal inhibitory concentrations (MIC's) for the various test articles were determined by standard solution broth methods,[4-6] using Mueller Hinton Broth (Difco; Catalog No. 275730). Bacteria for testing were obtained from ATCC and the following strains were used (*E. coli,* 25922; *S. enteric*, 6539; MRSA, 43300; *P. aeuginosa*, 27583; *K. pneumonia,* 700603; *E. faecium*, 700221; *A. baumanii*, BAA-747)

Titrations

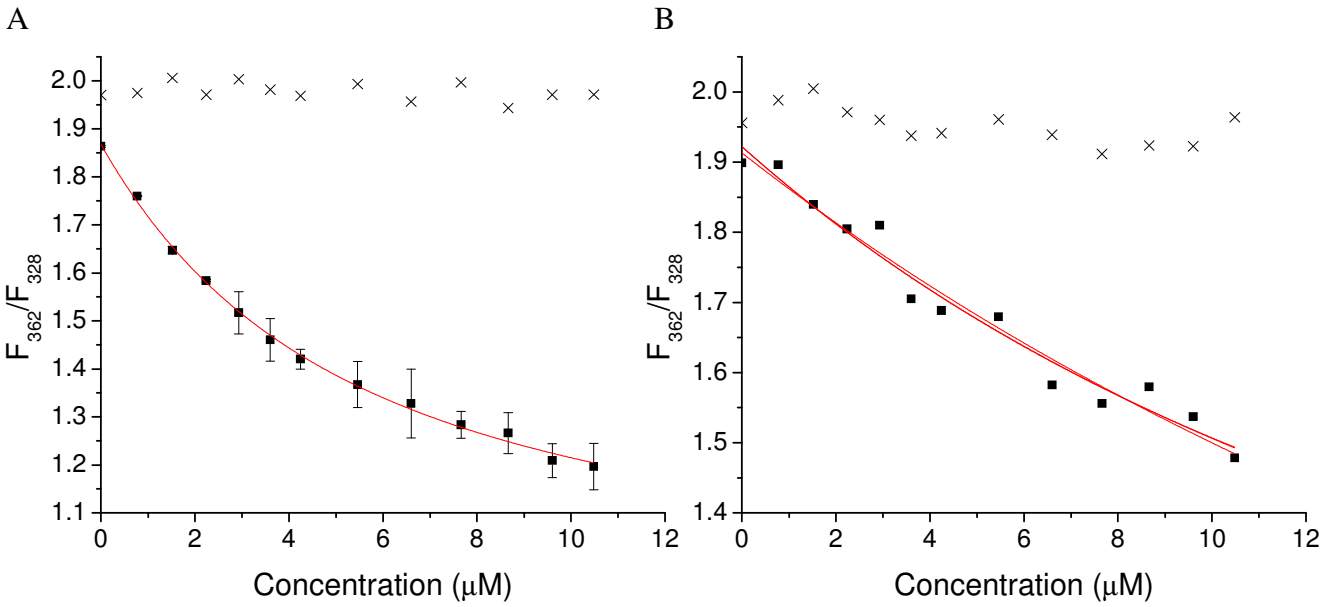

Figure SM1. Titrations of (A) peptide WRWYCR and (B) free tryptophan with (■) pUC19 plasmid DNA or (×) with the same volume of buffer lacking DNA. Titrations were monitored by the ratio (F_{362}/F_{328}) of fluorescence intensities at 362 and 328 nm, which provided a measure of the blue-shift in Trp fluorescence upon DNA binding. Titrations were performed at 37 °C in a buffer consisting of 20 mM HEPES, 100 mM NaCl, 1 mM TCEP, pH 7.

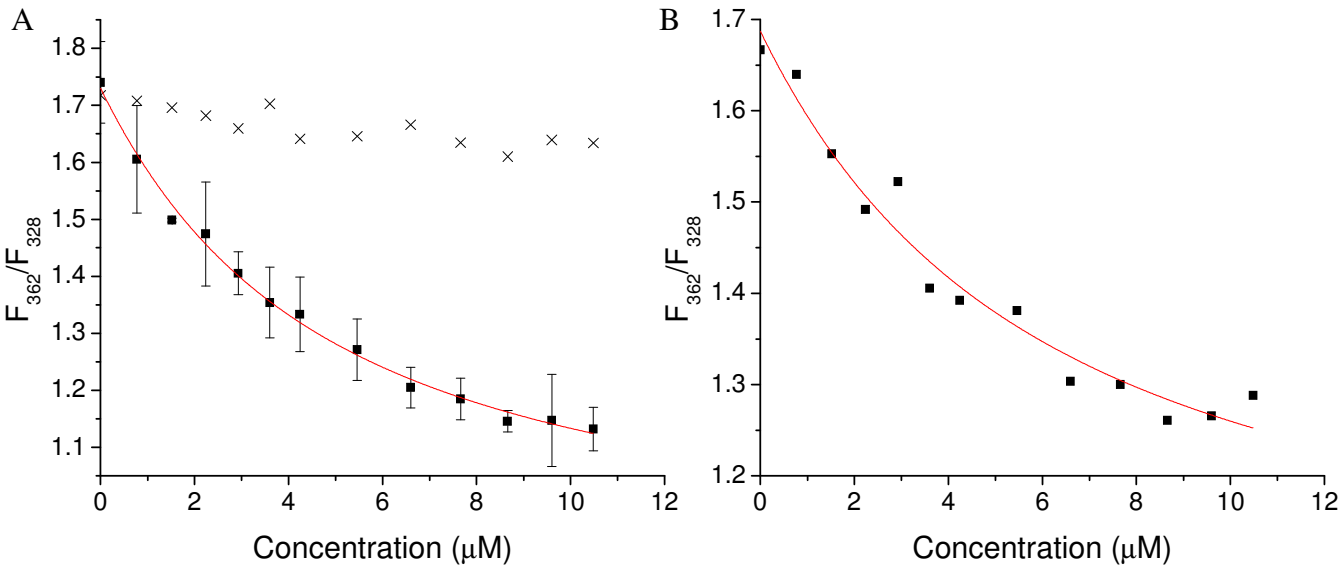

Figure SM2. Titrations of (A) complex Cu-GGHGWRWYCR and (B) peptide GGHGWRWYCR with (■) pUC19 plasmid DNA or (×) with the same volume of buffer lacking DNA. Titrations were monitored by the ratio (F_{362}/F_{328}) of fluorescence intensities at 362 and 328 nm, which provided a measure of the blue-shift in Trp fluorescence upon DNA binding. Titrations were performed at 37 °C in a buffer consisting of 20 mM HEPES, 100 mM NaCl, 1 mM TCEP, pH 7.

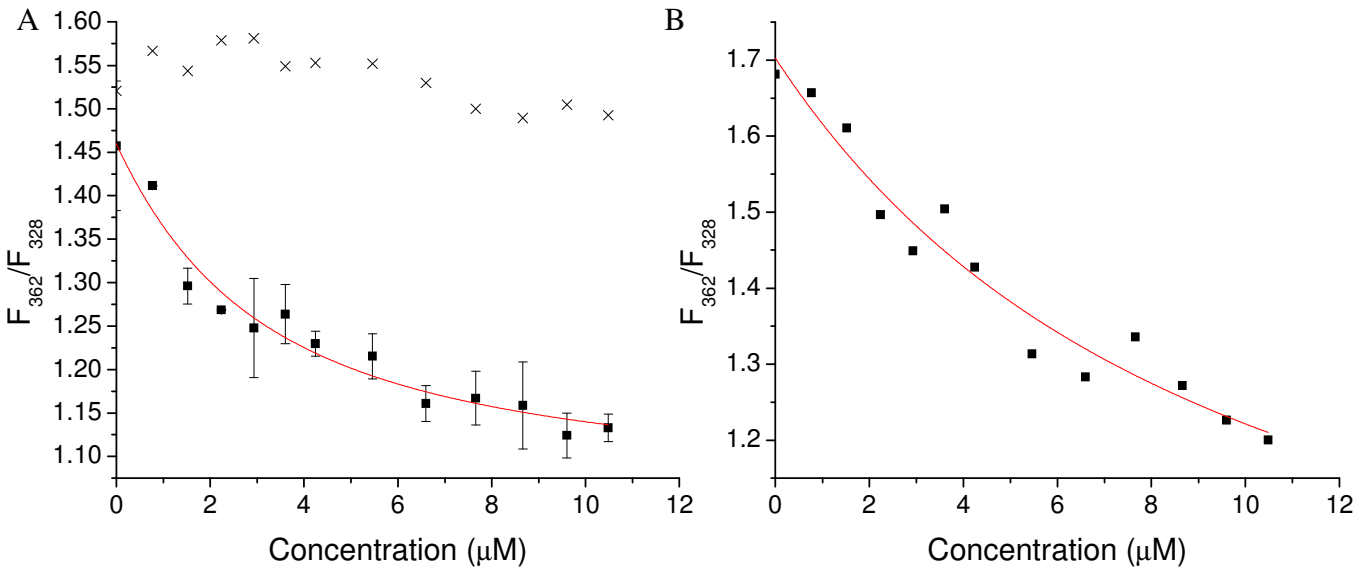

Figure SM3. Titrations of (A) complex Cu-GGHWRWYCRGGK and (B) peptide GGHWRWYCRGGK with (■) pUC19 plasmid DNA or (×) with the same volume of buffer lacking DNA. Titrations were monitored by the ratio (F_{362}/F_{328}) of fluorescence intensities at 362 and 328 nm, which provided a measure of the blue-shift in Trp fluorescence upon DNA binding. Titrations were performed at 37 °C in a buffer consisting of 20 mM HEPES, 100 mM NaCl, 1 mM TCEP, pH 7.

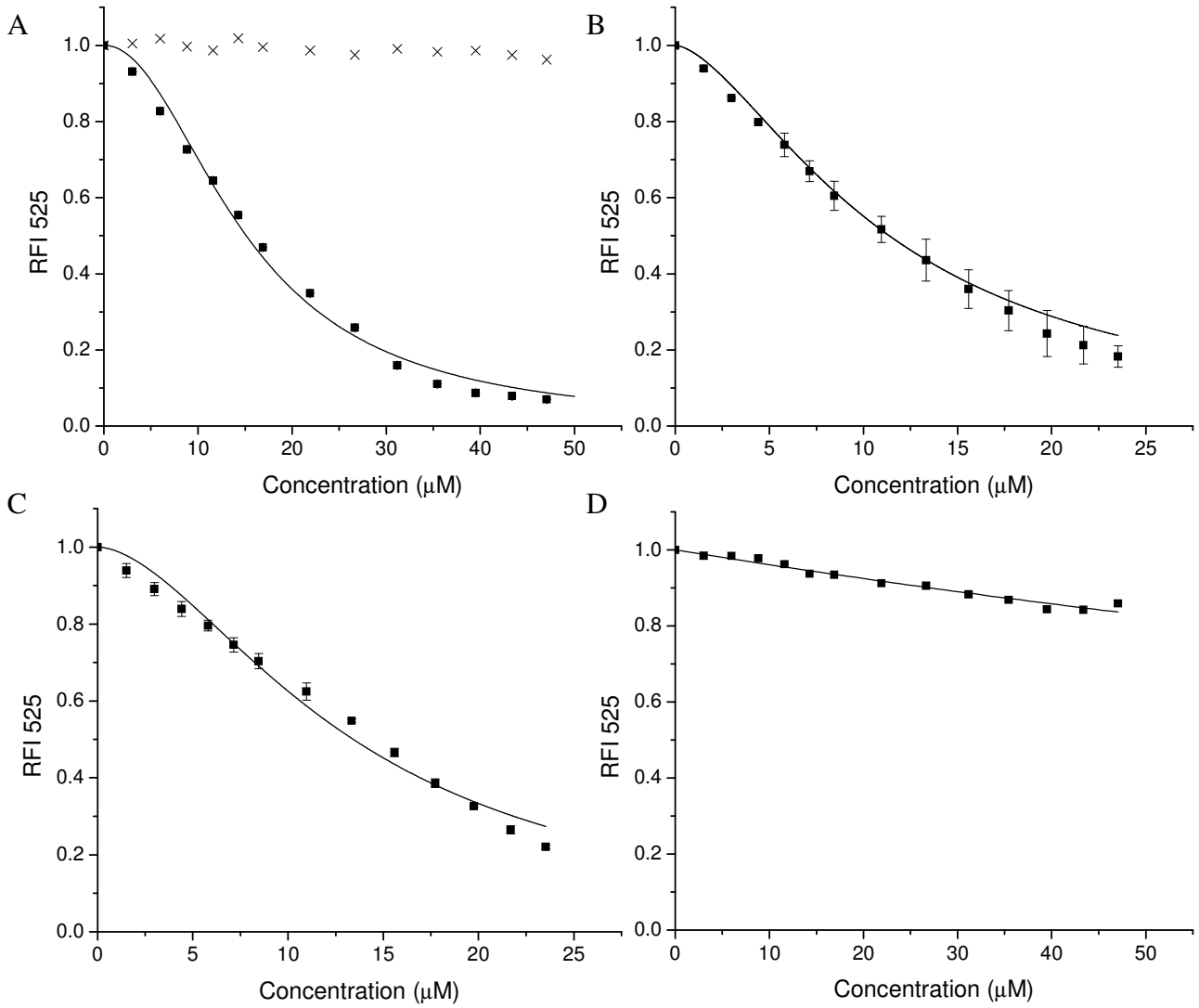

Figure SM4. Titrations of Fl-16S A-site RNA with (A) either (■) peptide WRWYCR or the (×) same volume of buffer lacking peptide, (B) complex Cu-GGHGWRWYCR, (C) complex Cu-GGHWRWYCRGGK, and (D) complex Cu-GGH. Titrations were monitored by following the fluorescence intensity at 525 nm, which provided a measure of the change in microenvironment upon binding of each peptide. Titrations with either Cu-GGH or buffer did not provide a significant fluorescence response. Titrations were performed at 37 °C in a buffer consisting of 20 mM HEPES, 100 mM NaCl, 1 mM TCEP, pH 7.

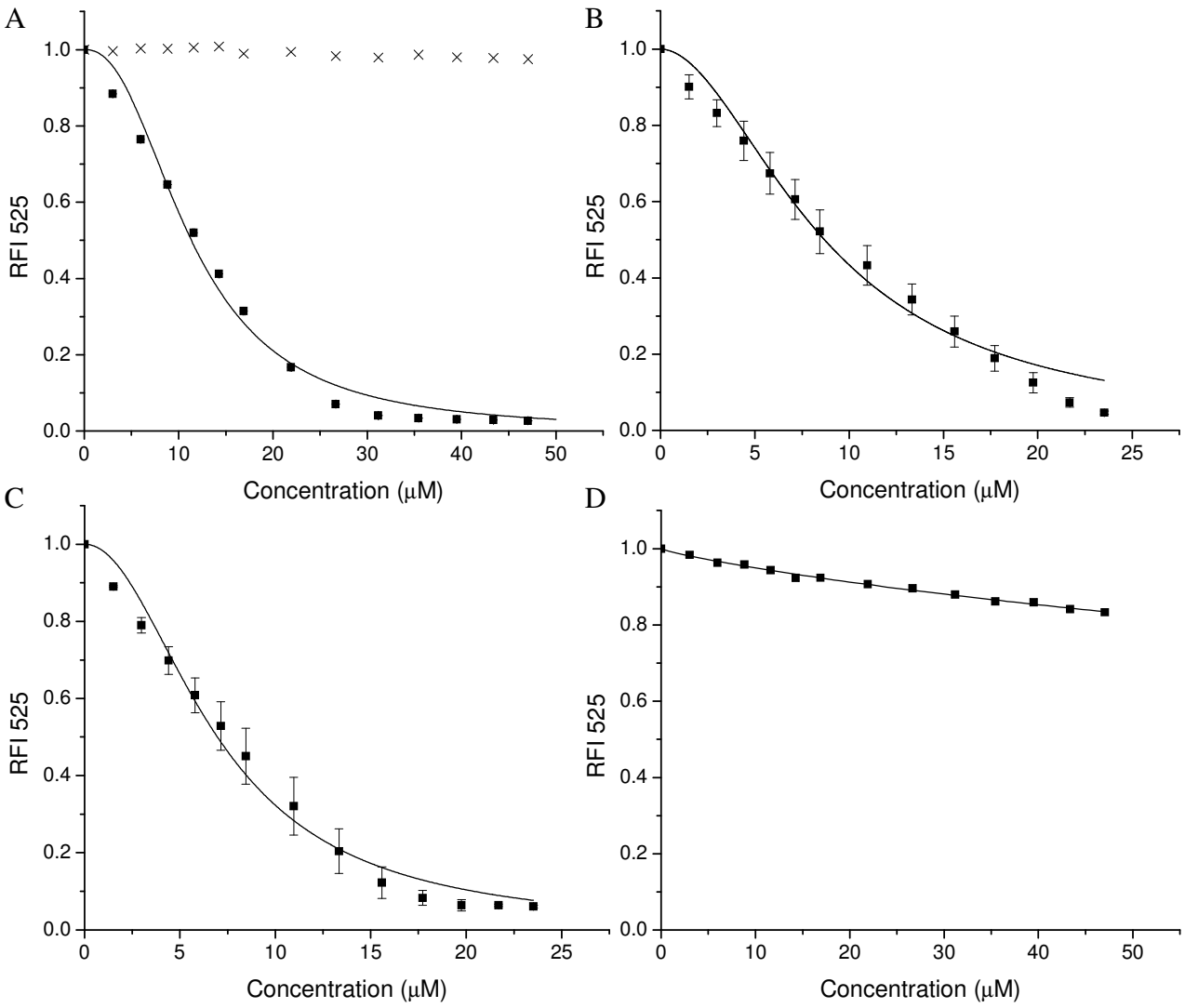

Figure SM5. Titrations of Fl-RRE IIB RNA with (A) either (■) peptide WRWYCR or the (×) same volume of buffer lacking peptide, (B) complex Cu-GGHGWRWYCR, (C) complex Cu-GGHWRWYCRGGK, and (D) complex Cu-GGH. Titrations were monitored by following the fluorescence intensity at 525 nm, which provided a measure of the change in microenvironment upon binding of each peptide. Titrations with either Cu-GGH or buffer did not provide a significant fluorescence response. Titrations were performed at 37 °C in a buffer consisting of 20 mM HEPES, 100 mM NaCl, 1 mM TCEP, pH 7.

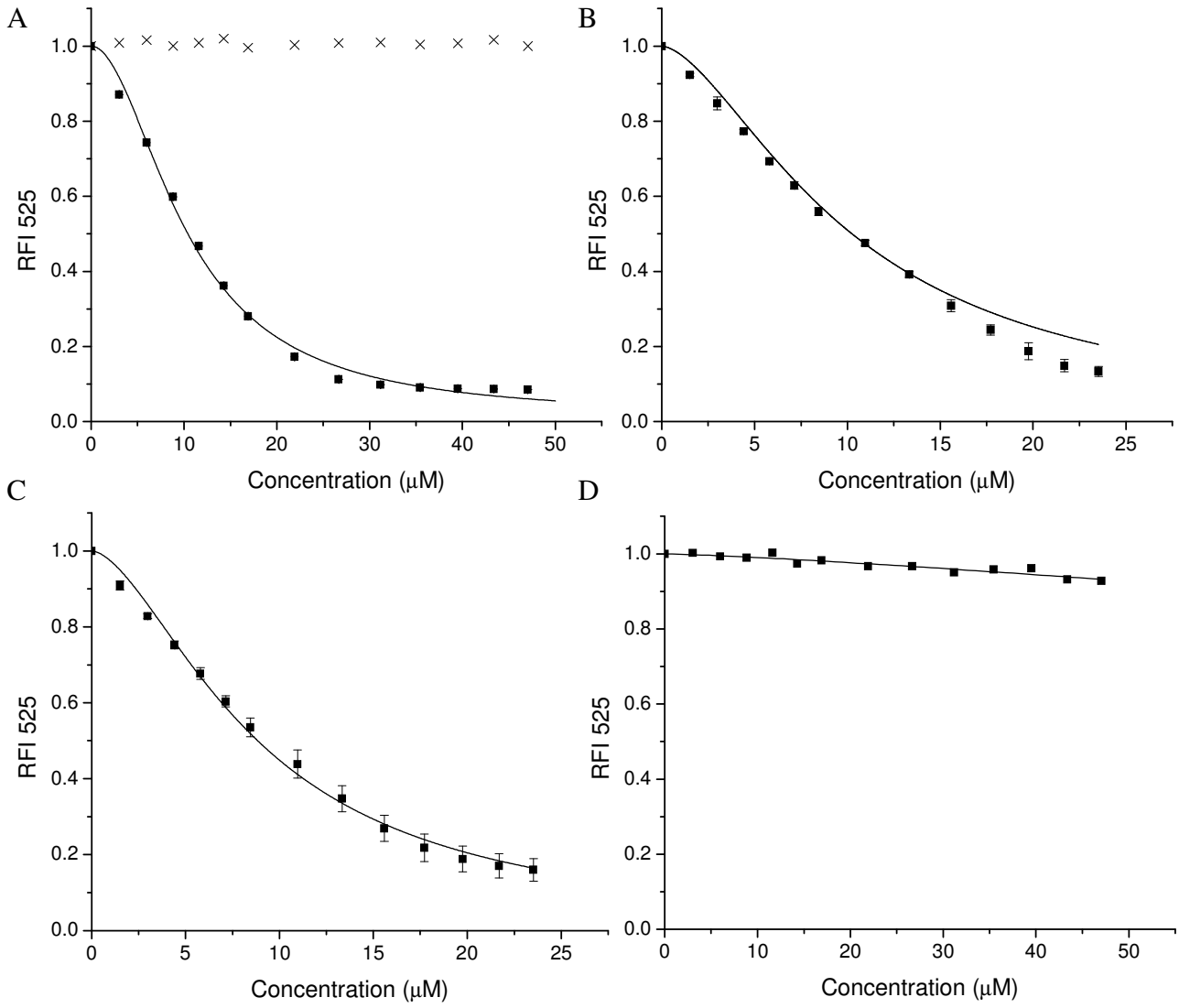

Figure SM6. Titrations of Fl-HCV IIB RNA with (A) either (■) peptide WRWYCR or the (×) same volume of buffer lacking peptide, (B) complex Cu-GGHGWRWYCR, (C) complex Cu-GGHWRWYCRGGK, and (D) complex Cu-GGH. Titrations were monitored by following the fluorescence intensity at 525 nm, which provided a measure of the change in microenvironment upon binding of each peptide. Titrations with either Cu-GGH or buffer did not provide a significant fluorescence response. Titrations were performed at 37 °C in a buffer consisting of 20 mM HEPES, 100 mM NaCl, 1 mM TCEP, pH 7.

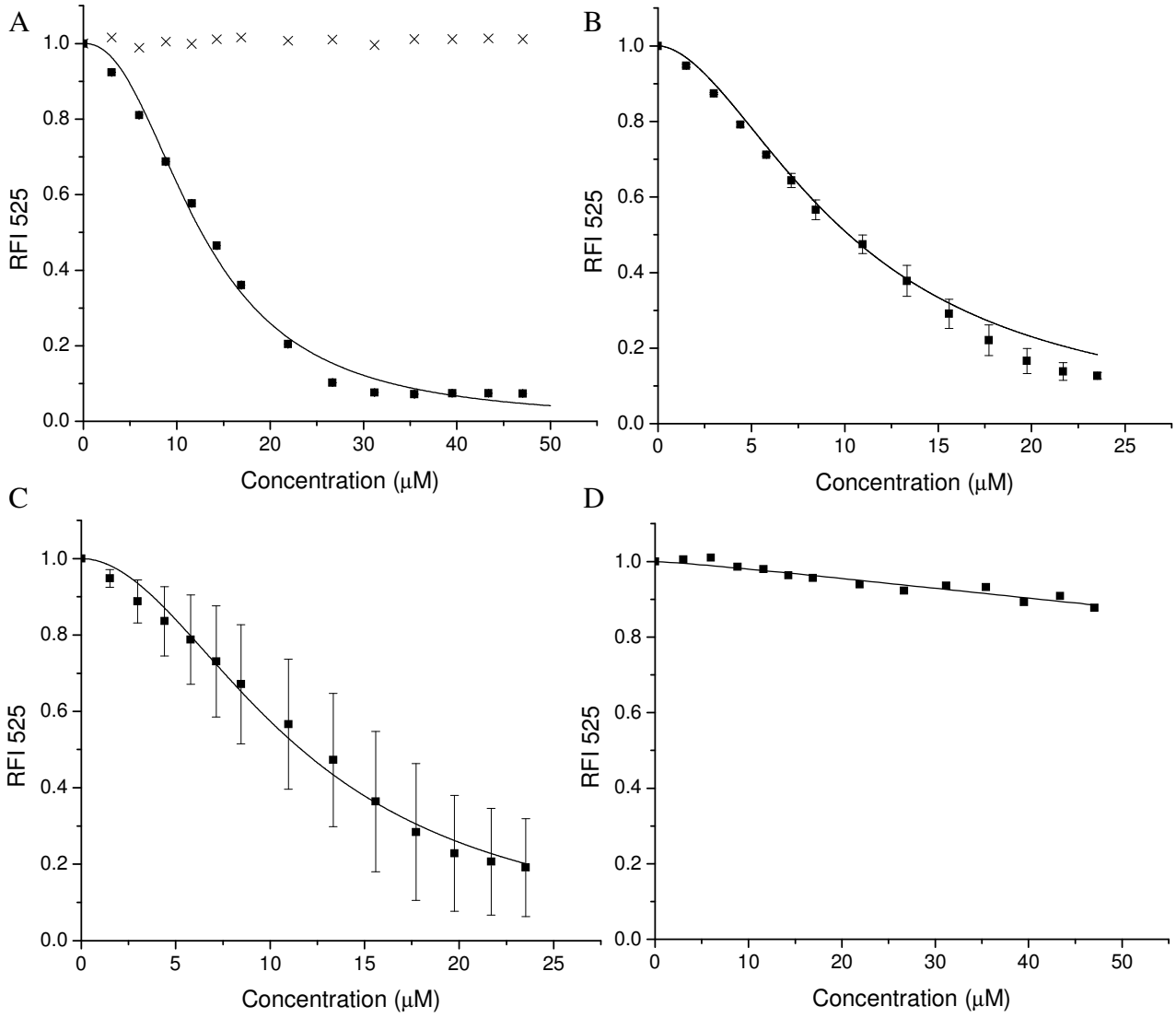

Figure SM7. Titrations of Fl-HCV IV RNA with (A) either (■) peptide WRWYCR or the (×) same volume of buffer lacking peptide, (B) complex Cu-GGHGWRWYCR, (C) complex Cu-GGHWRWYCRGGK, and (D) complex Cu-GGH. Titrations were monitored by following the fluorescence intensity at 525 nm, which provided a measure of the change in microenvironment upon binding of each peptide. Titrations with either Cu-GGH or buffer did not provide a significant fluorescence response. Titrations were performed at 37 °C in a buffer consisting of 20 mM HEPES, 100 mM NaCl, 1 mM TCEP, pH 7.

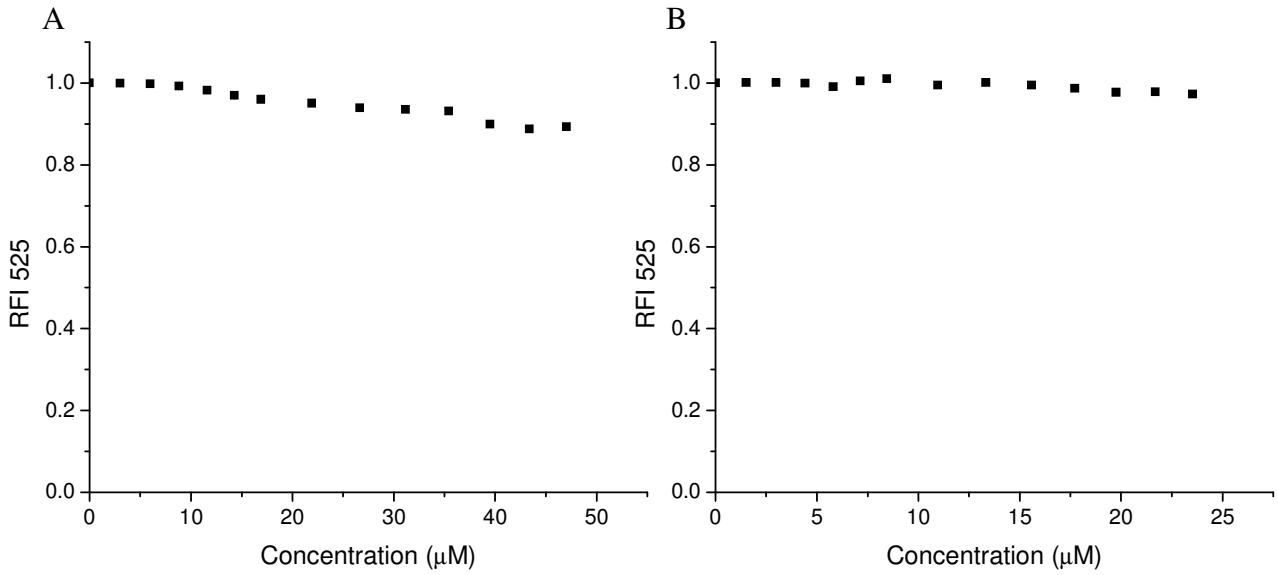

Figure SM8. Control titrations of free fluorescein lacking attached RNA with (A) peptide WRWYCR and (B) complex Cu-GGHGWRWYCR. No binding was observed between free fluorescein and peptide, indicating that the observed fluorescence responses in Fl-RNA titrations were indeed between RNA and peptide/complex. Titrations were performed at 37 °C in a buffer consisting of 20 mM HEPES, 100 mM NaCl, 1 mM TCEP, pH 7.

Reactions

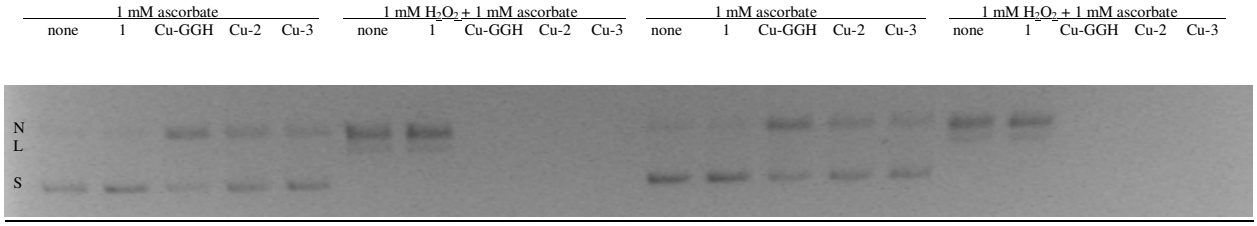

Form of plasmid DNA	Concentration of DNA base pairs (μM)									
	Co-reactant = 1 mM ascorbate					Co-reactants = 1 mM H_2O_2 and 1 mM ascorbate				
	none	1	Cu-GGH	Cu-2	Cu-3	none	1	Cu-GGH	Cu-2	Cu-3
Nicked	1.5 ± 0.1	1.20 ± 0.07	5.8 ± 0.1	3.2 ± 0.2	3.4 ± 0.1	7.6 ± 0.1	7.8 ± 0.1	0.0 ± 0.1	0.0 ± 0.2	0.0 ± 0.6
Linear	0.37 ± 0.01	0.5 ± 0.3	0.28 ± 0.03	0.5 ± 0.2	0.7 ± 0.2	1.95 ± 0.06	1.5 ± 0.2	0.0 ± 0.5	0.0 ± 0.3	0.0 ± 0.8
Supercoiled	8.2 ± 0.1	8.3 ± 0.4	3.9 ± 0.2	6.3 ± 0.4	5.92 ± 0.09	0.5 ± 0.2	0.64 ± 0.09	0.0 ± 0.7	0.0 ± 0.6	0.0 ± 0.4
Sum	10 ± 0	11.0 ± 0.5	11 ± 1	11 ± 2	11 ± 2	12 ± 2	12 ± 3	0 ± 1	0 ± 1	0 ± 1

Figure SM9. Cleavage of pUC19 plasmid DNA by no complex (none), 100 nM peptide WRWYCR-NH_2 (1), Cu-GGH, Cu-GGHGWRWYCR-NH_2 (Cu-2), and Cu-GGHWRWYCRGGK-NH_2 (Cu-3), in the presence of either 1 mM ascorbate or 1 mM H_2O_2 + 1 mM ascorbate. Upon cleavage, plasmid DNA was first converted from supercoiled (S) to nicked (N), and then to linearized (L) DNA. The 'Sum' reflects the sum of supercoiled, nicked, and linear forms of plasmid DNA. Incubations were performed for 4 h at 37 °C in a buffer consisting of 20 mM HEPES, 100 mM NaCl, pH 7. Initial concentrations were 10 μM base pairs DNA, 0.1 μM complex, and 1 mM each co-reactant.

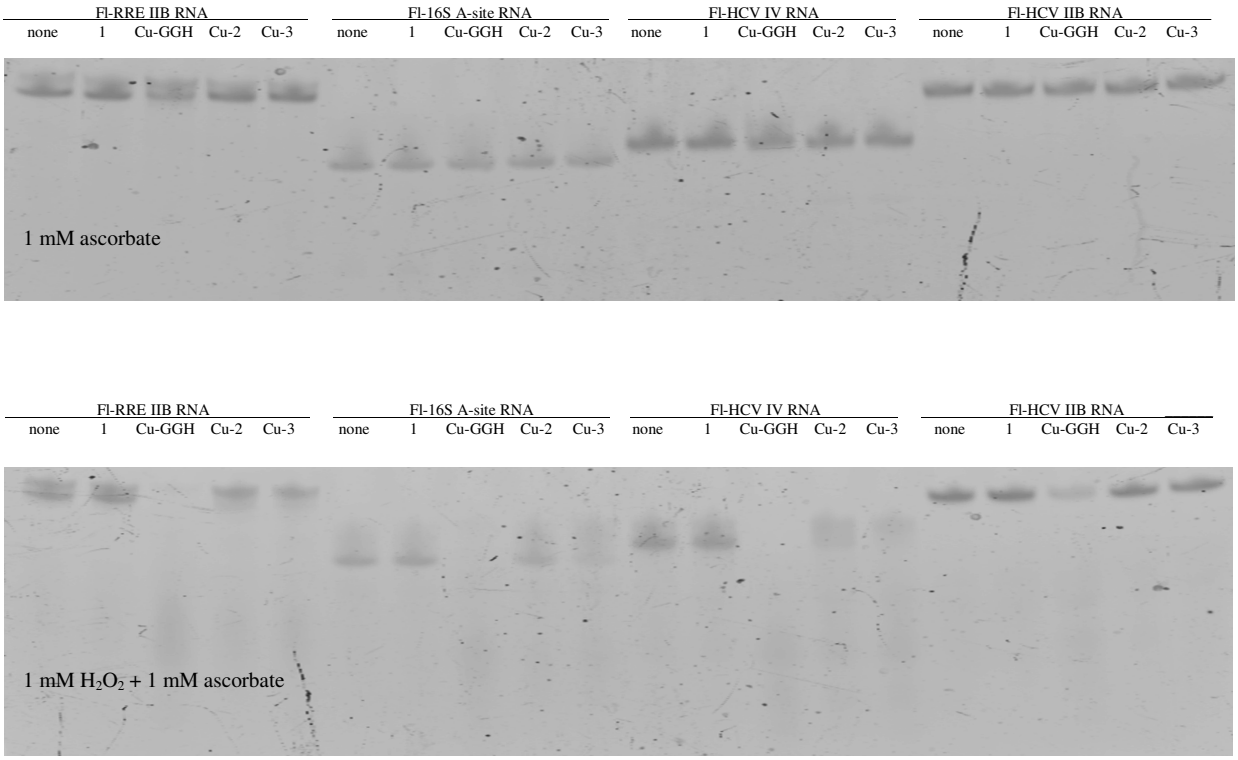

RNA	Concentration of RNA (μM)									
	Co-reactant = 1 mM ascorbate					Co-reactants = 1 mM H2O2 and 1 mM ascorbate				
	none	1	Cu-GGH	Cu-2	Cu-3	none	1	Cu-GGH	Cu-2	Cu-3
Fl-RRE IIB RNA	1	1.143483	0.926027	0.976738	0.954345	1	1.01391	0.131903	0.693342	0.459317
Fl-16S A-site RNA	1	1.064293	0.95118	1.049997	0.866095	1	0.925385	0.186023	0.874869	0.701111
Fl-HCV IV RNA	1	0.920801	0.88192	0.81945	0.775937	1	0.844884	0.023702	0.423467	0.314143
Fl-HCV IIB RNA	1	0.947847	0.922718	0.969793	0.95283	1	1.024715	0.333975	0.912769	0.92981

Figure SM10. Cleavage of each 5'-fluorescein-labeled RNA by no complex (none), 100 nM peptide WRWYCR-NH_2 (1), Cu-GGH, Cu-GGHGWRWYCR-NH_2 (Cu-2), and Cu-GGHWRWYCRGGK-NH_2 (Cu-3), in the presence of either 1 mM ascorbate or 1 mM H_2O_2 + 1 mM ascorbate. Incubations were performed for 5.5 h at 37 °C in a buffer consisting of 20 mM HEPES, 100 mM NaCl, pH 7. Initial concentrations were 1 μM RNA, 1 μM complex, and 1 mM each co-reactant.

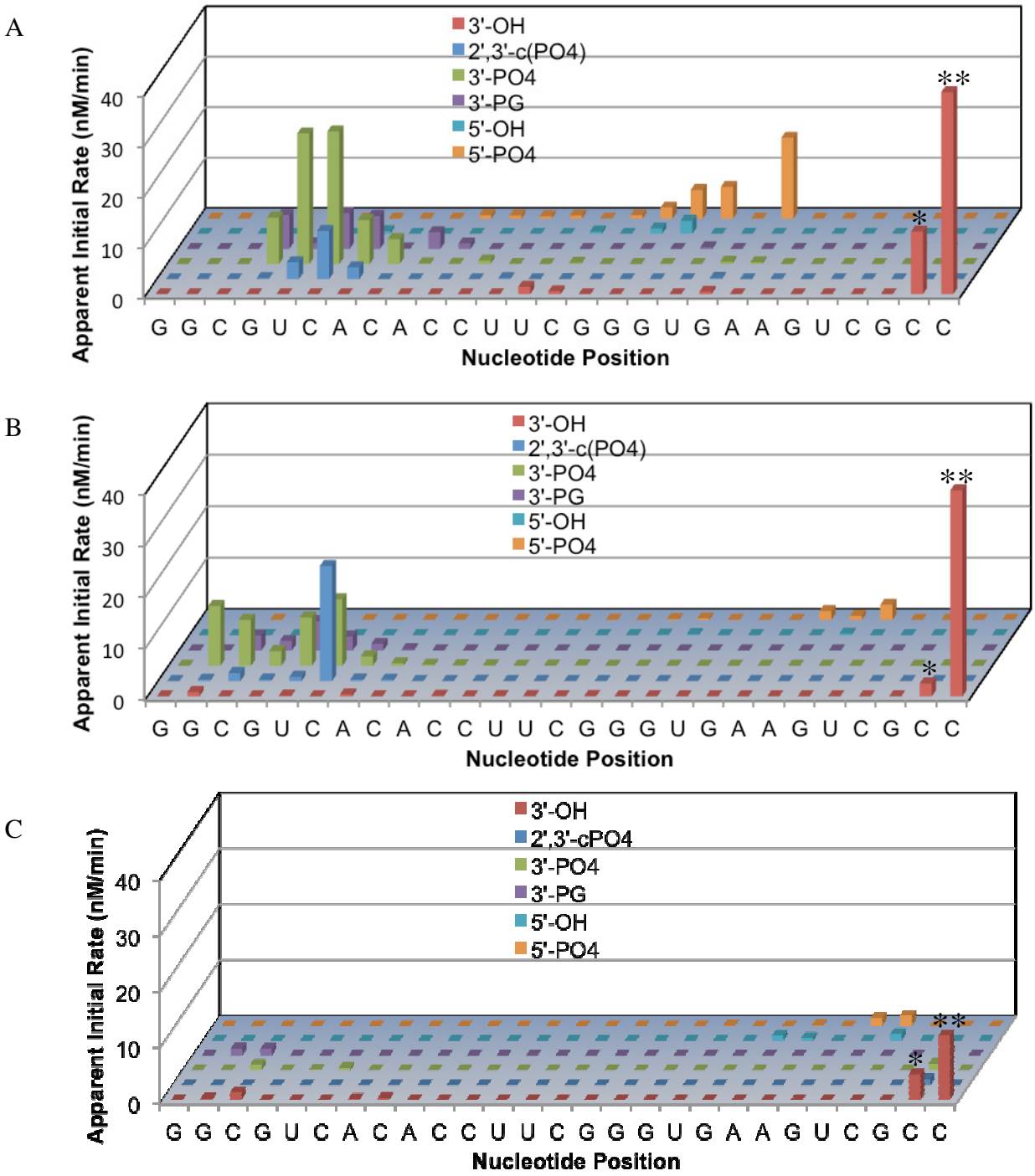

Figure SM11. MALDI-TOF mass spectrometry analysis of cleavage of 10 µM Fl-16S A-site RNA by (A) 10 µM Cu-GGH, (B) 10 µM Cu-GGHGWRWYCR, and (C) no complex, each in the presence of 1 mM H_2O_2 and 1 mM ascorbate. Apparent initial rates of formation of RNA fragments containing the listed overhangs at the listed nascent termini are shown and were determined as previously described.[4] Apparent initial rates of disappearance of the full-length 27-mer Fl-16S RNA (**) and the 26-mer impurity (*) are also shown. The listed nascent overhangs are 3'-hydroxyl (3'-OH), 2',3'-cyclic phosphate (2',3'-cPO$_4$), 3'-phosphate (3'-PO$_4$), 3'-phosphoglycolate (3'-PG), 5'-hydroxyl (5'-OH), and 5'-phosphate (5'-PO$_4$). Mass spectra for time-dependent incubations are shown in the following figures.

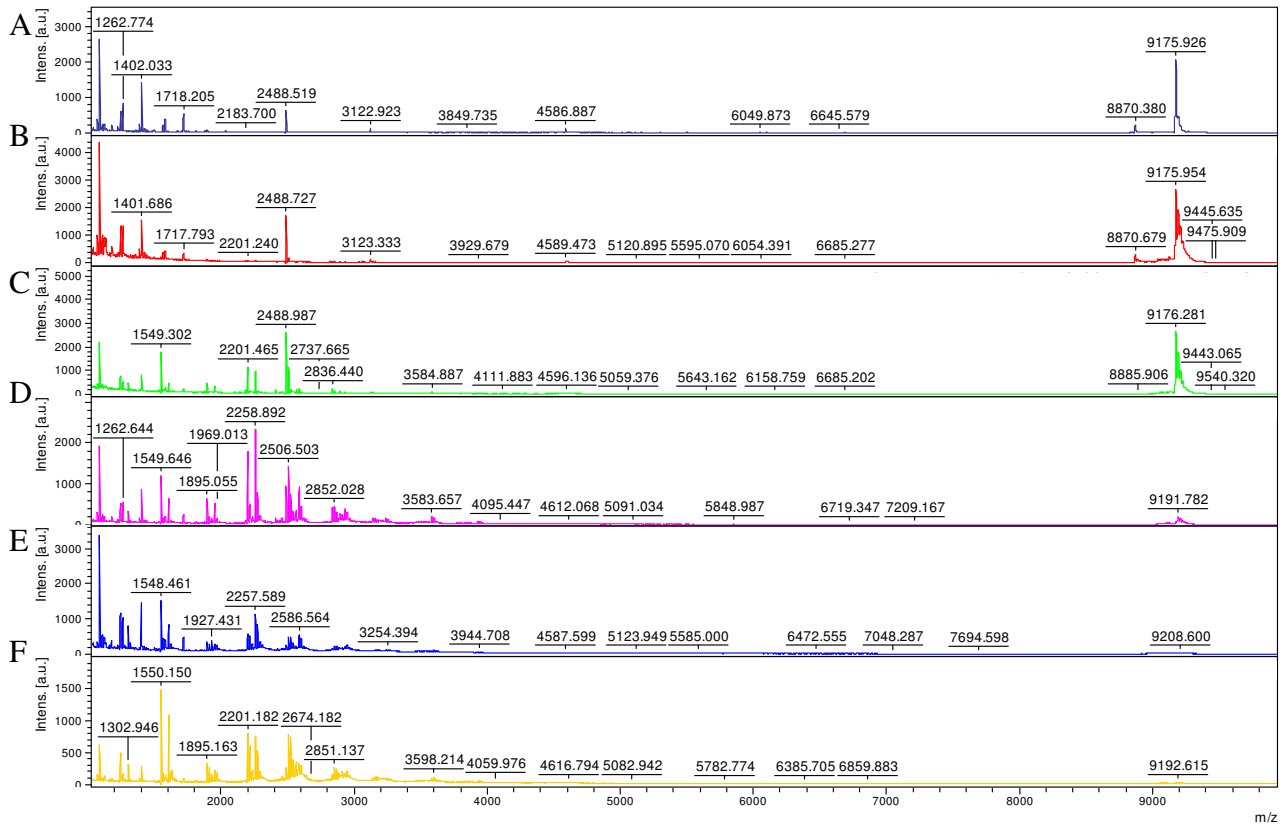

Figure SM12. MALDI-TOF mass spectra for time-dependent incubations of 10 µM Cu-GGH, 1 mM H_2O_2/ascorbate, and 10 µM Fl-16S A-site RNA at 37 ºC. (A) 0 min; (B) 15 min; (C) 30 min; (D) 60 min; (E) 90 min; (F) 120 min. The apparent rates of formation of individual RNA cleavage fragments were obtained from these data and are summarized in Figure SM11. Expected masses used for identification of products are shown in Table SM1. All peak mass matching required that the expected and observed masses matched within 200 ppm.

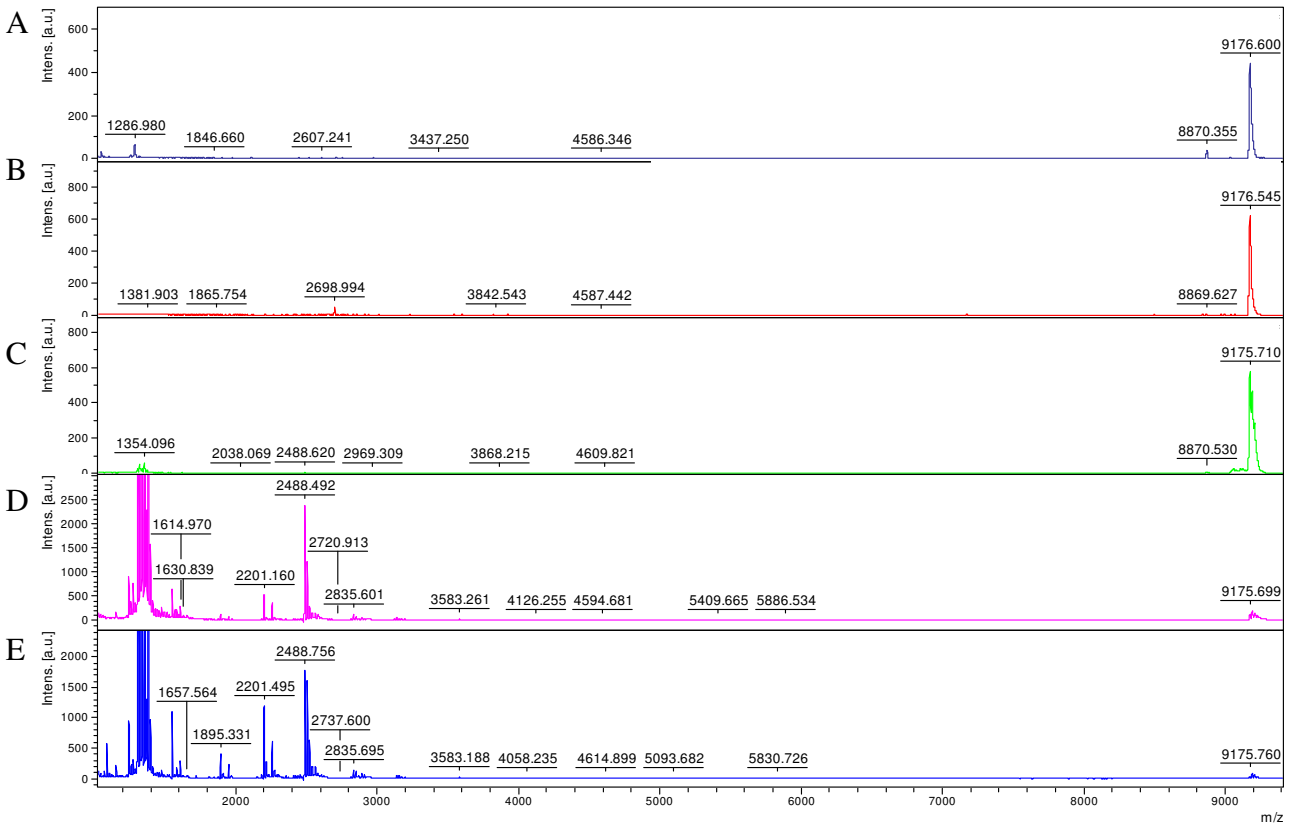

Figure SM13. MALDI-TOF mass spectra for time-dependent incubations of 10 µM Cu-GGHGWRWYCR, 1 mM H_2O_2/ascorbate, and 10 µM Fl-16S A-site RNA at 37 ºC. (A) 0 min; (B) 10 min; (C) 40 min; (D) 90 min; (E) 120 min. The apparent rates of formation of individual RNA cleavage fragments were obtained from these data and are summarized in Figure SM11. Expected masses used for identification of products are shown in Table SM1. All peak mass matching required that the expected and observed masses matched within 200 ppm.

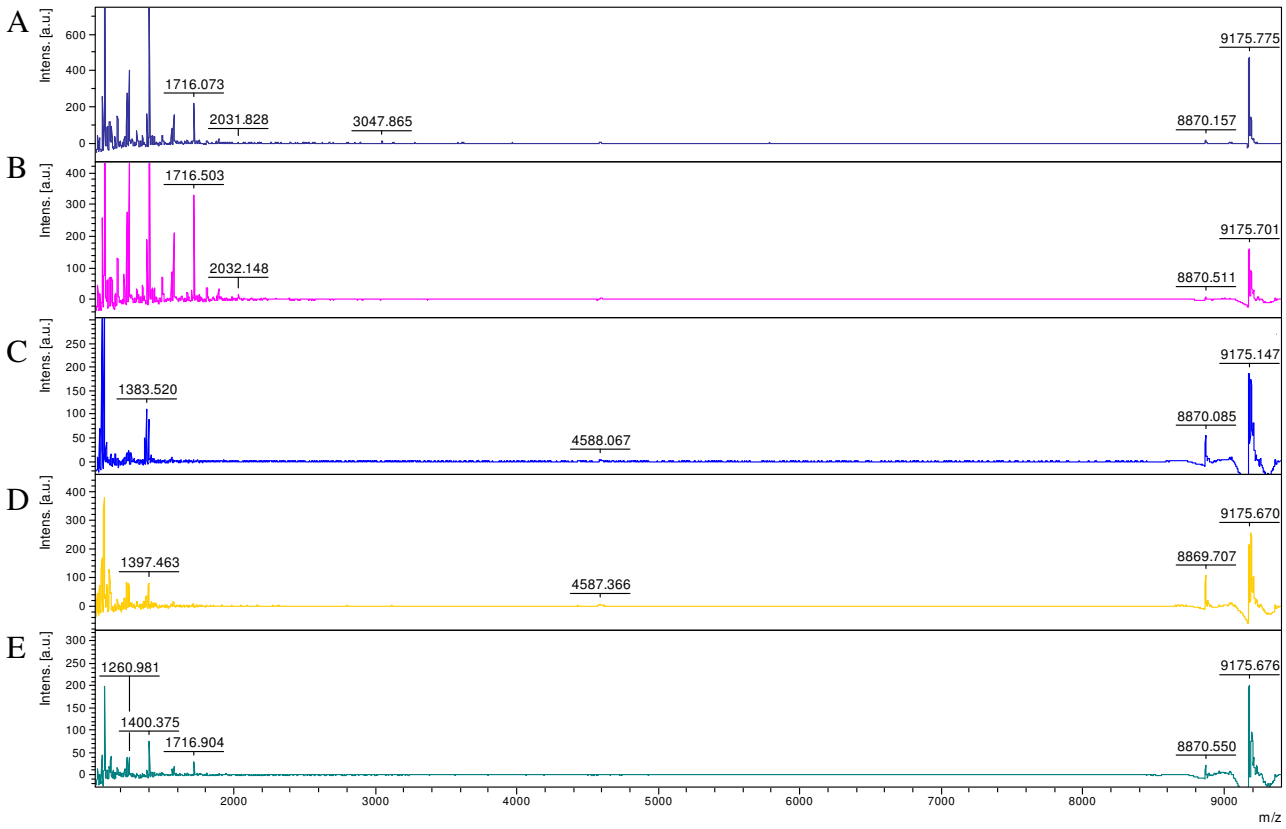

Figure SM14. MALDI-TOF mass spectra for time-dependent incubations of 1 mM H_2O_2/ascorbate (no catalyst), and 10 µM Fl-16S A-site RNA at 37 ºC. (A) 0 min; (B) 30 min; (C) 40 min; (D) 90 min; (E) 120 min. The apparent rates of formation of individual RNA cleavage fragments were obtained from these data and are summarized in Figure SM11. Expected masses used for identification of products are shown in Table SM1. All peak mass matching required that the expected and observed masses matched within 200 ppm.

Nascent 3' Overhangs								Nascent 5' Overhangs			
3'-OH		2,3-cyclic phosphate		3'-phosphate		3'-phosphoglycolate		5'-OH		5'-phosphate	
m/z (Da)	nucl. pos.	m/z (Da)	nucl. pos.	m/z (Da)	nucl. pos.	m/z (Da)	nucl. pos.	m/z (Da)	nucl. pos.	m/z (Da)	nucl. pos.
9175.71	**27**										
8870.53	26	8932.49	26	8950.51	26	9008.55	26	8293.02	2	8373	2
8565.35	25	8627.31	25	8645.33	25	8703.37	25	7947.81	3	8027.79	3
8220.14	24	8282.1	24	8300.12	24	8358.16	24	7642.63	4	7722.61	4
7914.96	23	7976.92	23	7994.94	23	8052.98	23	7297.42	5	7377.4	5
7608.79	22	7670.75	22	7688.77	22	7746.81	22	6991.25	6	7071.23	6
7263.58	21	7325.54	21	7343.56	21	7401.6	21	6686.07	7	6766.05	7
6934.37	20	6996.33	20	7014.35	20	7072.39	20	6356.86	8	6436.84	8
6605.16	19	6667.12	19	6685.14	19	6743.18	19	6051.68	9	6131.66	9
6259.95	18	6321.91	18	6339.93	18	6397.97	18	5722.47	10	5802.45	10
5953.78	17	6015.74	17	6033.76	17	6091.8	17	5417.29	11	5497.27	11
5608.57	16	5670.53	16	5688.55	16	5746.59	16	5112.11	12	5192.09	12
5263.36	15	5325.32	15	5343.34	15	5401.38	15	4805.94	13	4885.92	13
4918.15	14	4980.11	14	4998.13	14	5056.17	14	4499.77	14	4579.75	14
4612.97	13	4674.93	13	4692.95	13	4750.99	13	4194.58	15	4274.56	15
4306.8	12	4368.76	12	4386.78	12	4444.82	12	3849.37	16	3929.35	16
4000.63	11	4062.59	11	4080.61	11	4138.65	11	3504.16	17	3584.14	17
3695.45	10	3757.41	10	3775.43	10	3833.47	10	**3158.95**	**18**	3238.93	18
3390.26	9	3452.22	9	3470.24	9	3528.28	9	2852.78	19	2932.76	19
3061.05	8	**3123.01**	**8**	3141.03	8	3199.07	8	2507.57	20	2587.55	20
2755.87	7	2817.83	7	2835.85	7	2893.89	7	2178.36	21	2258.34	21
2426.66	6	**2488.62**	**6**	2506.64	6	2564.68	6	1849.15	22	1929.13	22
2121.48	5	2183.44	5	2201.46	5	2259.5	5	1503.94	23	1583.92	23
1815.31	4	**1877.27**	**4**	1895.29	4	1953.33	4	1197.77	24	1277.75	24
1470.1	3	1532.06	3	1550.08	3	1608.12	3	892.59	25	972.57	25
1164.92	2	**1226.88**	**2**	1244.9	2	1302.94	2	547.38	26	627.36	26
819.71	1	881.67	1	899.69	1	957.73	1	242.2	27	322.18	27

Table SM1. Predicted masses for products ions (z = -1) resulting from cleavage of Fl-16S A-site RNA (27-mer). The predicted masses shown here correspond to $[RNA]^{1-}$ fragments terminated with one of the listed nascent overhangs, at one of the positions shown. These masses were used for assignment of peaks in mass spectra. All fragments with nascent 3' overhangs were terminated at the 5' end with fluorescein; all fragments with nascent 5' overhangs were terminated at the 3' end with a 3'-hydroxyl group. The Fl-16S RNA is similarly terminated at the 5' end with fluorescein and at the 3' end with a 3'-hydroxyl group (unreacted; m/z = 9175.71 Da). Peaks used for internal calibration are shown in bold (also included $[Fl\text{-}16S - 2H]^{2-}$ with m/z = 4587.35 Da).

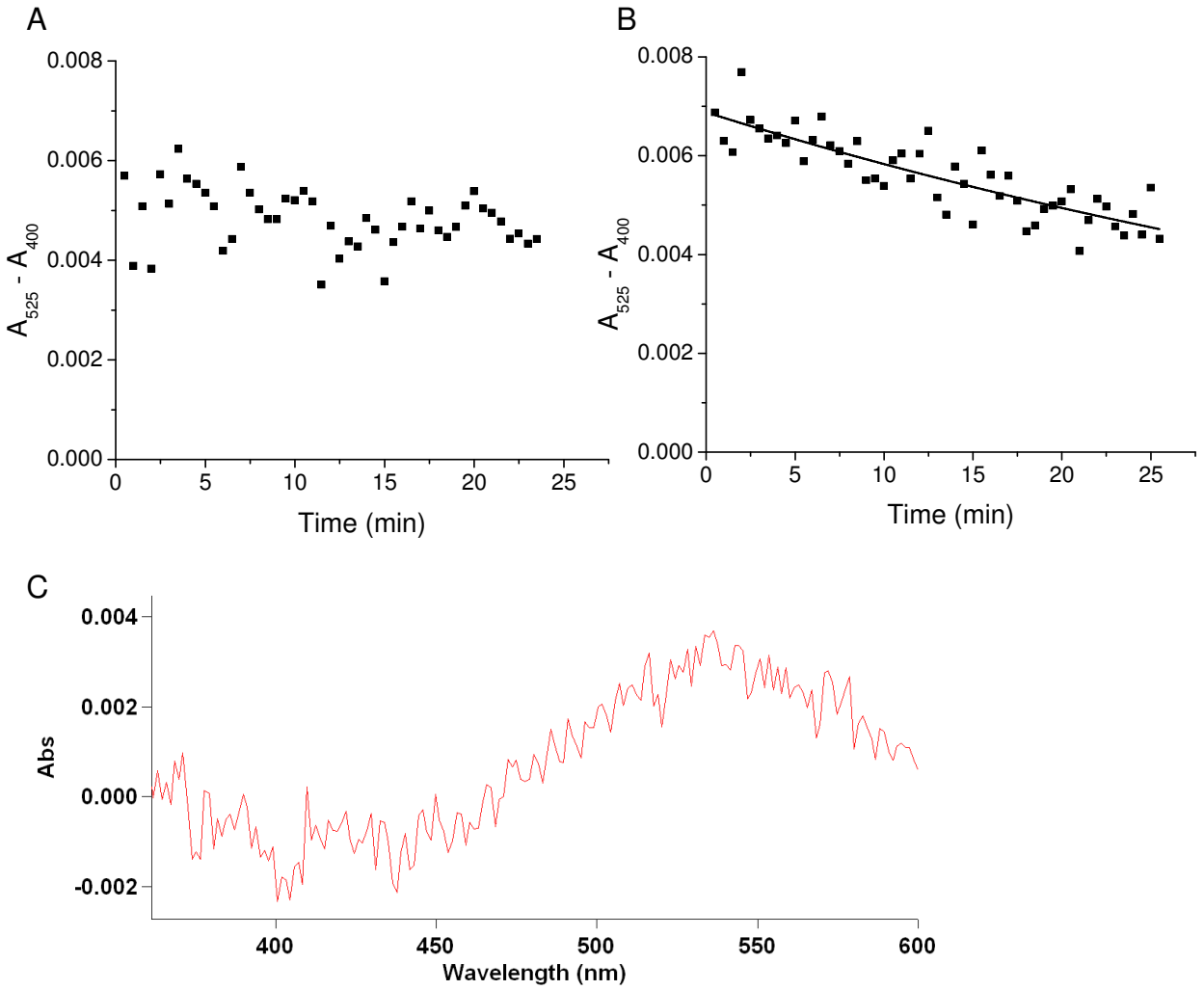

Figure SM15. TCEP did not interfere with the formation or kinetic stability of Cu-GGH under the conditions used in nucleic acid-binding experiments (TCEP was added in nucleic acid-binding experiments with the purpose of reducing any disulfide bonds in the extended peptides). (A) Complex Cu-GGH (100 µM) was allowed to form in the presence of 1 mM TCEP, and Cu-GGH complex formation was rapid (complete within < 0.5 min), as seen by the signature absorbance peak of Cu-GGH near 525 nm (minus the background absorbance at 400 nm). (B) In a complementary experiment, TCEP (1 mM) was added to pre-formed 100 µM Cu-GGH, and the complex remained stable (only a slight red-shift in the absorbance peak maximum was seen, from 525 nm to 533 nm, which accounts for the slight apparent decrease in absorbance at 525 nm shown above). This subtle change may have been due to a non-destabilizing weak axial coordination of TCEP to the non-chelated axial coordination sites of Cu-GGH (sites usually occupied by H_2O or co-reactants), although such weak coordination is unlikely to affect reactivity, and the apparent second order rate constant for this change was only 17 $M^{-1}min^{-1}$ (insignificant for the binding experiments containing 1 mM TCEP). The trace in (C) shows the absorbance of complex Cu-GGH in the presence of 1 mM TCEP (maximum near 533 nm) and was obtained 10 min after mixing 100 µM $CuCl_2$ and 200 µM GGH in presence of 1 mM TCEP. A separate mixture of 100 µM $CuCl_2$ and 1 mM TCEP (without GGH) showed no absorbance near 525 or 533 nm. Experiments were performed in buffer of 20 mM HEPES, 100 mM NaCl, pH 7, at 37 ºC.

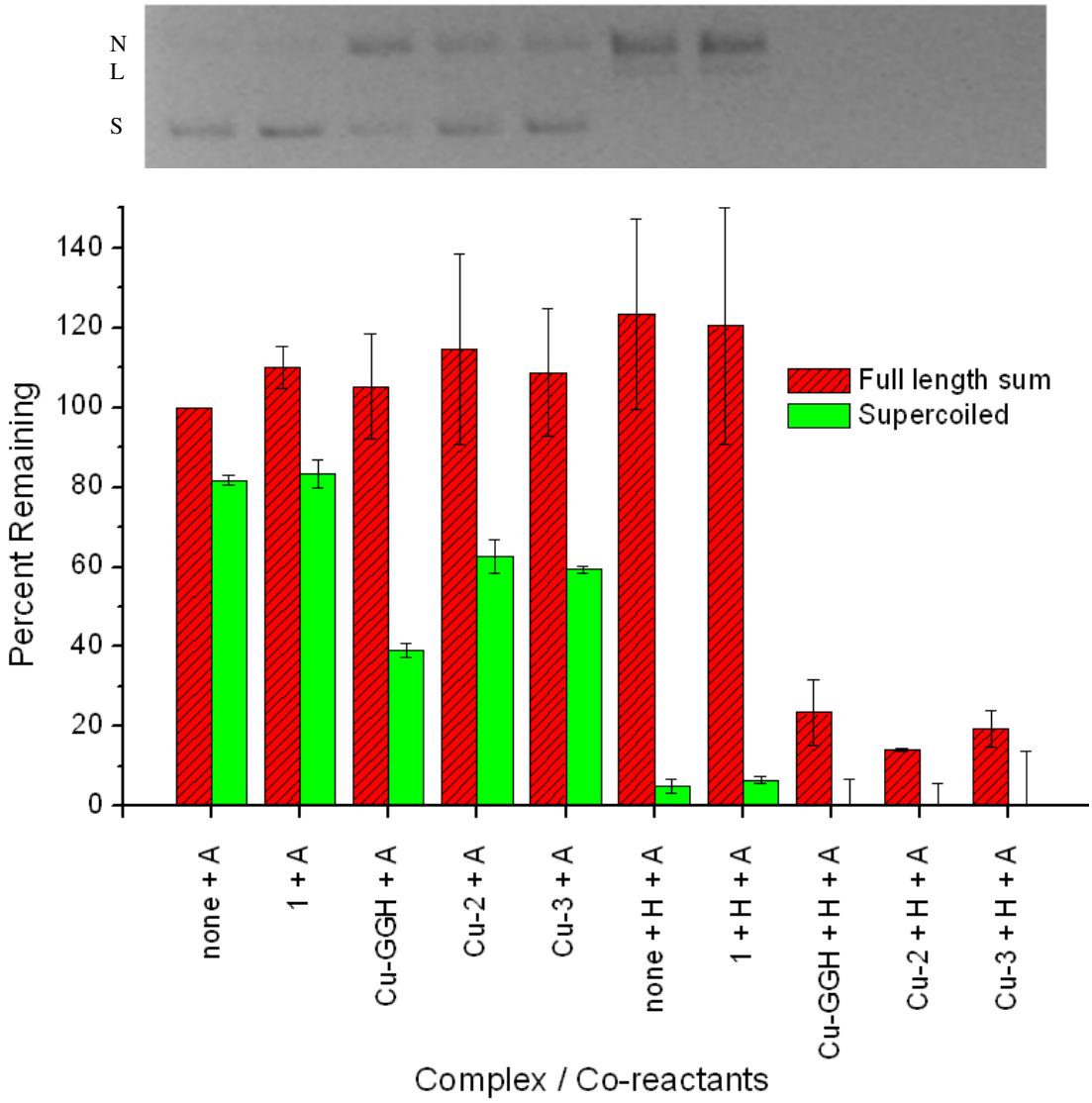

Figure SM16. Nicking and total cleavage of plasmid DNA by each metallopeptide, in the presence of co-reactants. The gel above corresponds to the data in the bar plot below (average of duplicate trials). After 4 h incubation, cleavage resulted in nicking of plasmid DNA, followed by linearization, and finally to a distribution of smaller fragments (not shown above). Initial concentrations were 10 μM base pairs DNA (defined as 100%), 0.1 μM complex, and 1 mM each co-reactant. 'Full length sum' is the sum of the percentages of supercoiled (S), nicked (N), and linear (L) forms of DNA.

SM References

1. J. C. Joyner and J. A. Cowan, *J. Am. Chem. Soc.*, 2011, **133**, 9912-9922.
2. J. C. Joyner, L. Hocharoen and J. A. Cowan, *J. Am. Chem. Soc.*, 2011, **134**, 3396–3410.
3. J. C. Joyner, K. D. Keuper and J. A. Cowan, *Dalton Trans.*, 2012, **41**, 6567-6578.
4. J. C. Joyner, K. Keuper and J. A. Cowan, *Nucl. Acids Res.*, 2012, **DOI: 10.1093/nar/gks811**.